*Pure Appl. Chem.*, Vol. 85, No. 11, pp. 2059–2076, 2013.
http://dx.doi.org/10.1351/PAC-CON-13-01-04


# Solubility phenomena in science and education: Experiments, thermodynamic analyses, and theoretical aspects*

Heinz Gamsjäger

*Lehrstuhl für Physikalische Chemie, Montanuniversität Leoben, A-8700 Leoben, Austria*

*Abstract*: Solubility equilibria between solid salts, salt hydrates, and water play an important role in fundamental and applied branches of chemistry. The continuous interest in this field has been reflected by the 15th International Symposium on Solubility Phenomena as well as by the ongoing IUPAC-NIST Solubility Data Series (SDS), which by now comprises close to 100 volumes.

Three typical examples concerning solubility phenomena of ionic solids in aqueous solutions are discussed: (1) sparingly soluble, simple molybdates; (2) sparingly soluble ionic solids with basic anions; and (3) hydrolysis of inert hexa-aqua-M(III) ions, where M is Ir, Rh, or Cr.

In the first two cases, essential experimental details are discussed, an outline of thermodynamic analyses is given, and theoretical aspects are emphasized. In the third case, an educational suggestion is made.

*Keywords*: chemical thermodynamics; chromium(III) hydrolysis; molybdates; nickel hydroxide; phase diagrams; solubility.

## THERMODYNAMIC ANALYSIS OF THE SOLUBILITY OF SPARINGLY SOLUBLE SIMPLE MOLYBDATES

Thermodynamic properties of molybdates are of continuous interest in reactor science because these compounds may form in irradiated fuel rods as a consequence of interactions between different fission-product oxides, see O'Hare [1]. Reliable thermodynamic data are the prerequisite for modelling of the chemical behavior of hazardous waste components. Thus, the standard Gibbs energy as well as the standard enthalpy of molybdate ion formation was studied systematically.

### Standard Gibbs energy and enthalpy of formation of aqueous molybdate ion $MoO_4^{2-}$

O'Hare et al. [2] derived $\Delta_f G°(MoO_4^{2-}, aq, 298.15\ K)$ from the solubility product of the sparingly soluble molybdates $BaMoO_4$, $SrMoO_4$, $CaMoO_4$, $Ag_2MoO_4$, and $FeMoO_4$, which dissociate as follows:

$$M_nMoO_4(cr) \rightleftharpoons nM^{2+/n}(aq) + MoO_4^{2-}(aq) \quad (1)$$

**Pure Appl. Chem.* **85**, 2027–2144 (2013). A collection of invited papers based on presentations at the 15th International Symposium on Solubility Phenomena and Related Equilibrium Processes (ISSP-15), Xining, China, 22–27 July 2012.

Standard Gibbs energy and standard enthalpy of molybdate ion formation, and standard entropy of molybdate ion are given by eqs. 2a–c.

$$\Delta_f G^{\ominus}(MoO_4^{2-}, aq) = \Delta_{sln} G^{\ominus} - n\Delta_f G^{\ominus}(M^{2+/n}, aq) + \Delta_f G^{\ominus}(M_n MoO_4, cr) \quad (2a)$$

$$\Delta_f H^{\ominus}(MoO_4^{2-}, aq) = \Delta_{sln} H^{\ominus} - n\Delta_f H^{\ominus}(M^{2+/n}, aq) + \Delta_f H^{\ominus}(M_n MoO_4, cr) \quad (2b)$$

$$S^{\ominus}(MoO_4^{2-}, aq) = \Delta_{sln} S^{\ominus} - nS^{\ominus}(M^{2+/n}, aq) + S^{\ominus}(M_n MoO_4, cr) \quad (2c)$$

Gibbs energy $\Delta_{sln}G^{\circ}$, enthalpy $\Delta_{sln}H^{\circ}$, and $\Delta_{sln}S^{\circ}$ of dissolution according to reaction 1 are related to the solubility product $K_{s0}^{\circ}$ by eqs. 3–5

$$\Delta_{sln} G^{\ominus} = -RT \ \ln K_{s0}^{\ominus} \quad (3)$$

$$\left[\frac{\partial \ln K_{s0}^{\ominus}}{\partial(1/T)}\right]_p = -\Delta_{sln} H^{\ominus} / R \quad (4)$$

$$\left[\frac{\partial(T \ln K_{s0}^{\ominus})}{\partial T}\right]_p = \Delta_{sln} S^{\ominus} / R \quad (5)$$

Clearly the solubility product at the reference temperature, usually 298.15 K, is the most reliable contribution solubility research can provide. It is, however, always worthwhile to evaluate equilibrium constants measured at various temperatures using eqs. 4 and 5 to check whether thermodynamic consistency prevails between data obtained by solubility, calorimetric, potentiometric, and other methods.

In this context the question arose: Have solubility measurements carried out since O'Hare's seminal paper [2] markedly changed our knowledge of $\Delta_f G^{\circ}$ ($MoO_4^{2-}$, aq) and $\Delta_f H^{\circ}$ ($MoO_4^{2-}$, aq)?

## Thermodynamic analysis of solubility data

The solubility of silver molybdate has been most thoroughly investigated, best of all simple, sparingly soluble metal molybdates. The corresponding data have been used for exemplifying thermodynamic solubility analysis. Eight references [3–10] have been found with experimental data that permit the determination of lg $K_{s0}^{\circ}$ according to the SIT approach at various temperatures, see eq. 6 [11,12].

$$\lg K_{s0}^{\ominus} = \lg\left(a_{Ag^+}^2 a_{MoO_4^{2-}}\right) = \lg\left(m_{Ag^+}^2 m_{MoO_4^{2-}}\right) - 6D + \Delta\varepsilon I_m \quad (6)$$

As $Ag_2MoO_4$(s) is sparingly soluble, the ionic strength $I_m$ of saturated solutions in pure water

$$m_{Ag^+} = 2m_{MoO_4^{2-}} \quad (7)$$

$$I_m = 3m_{MoO_4^{2-}} \quad (8)$$

is so low that the term $\Delta\varepsilon I_m$ with the unknown ion interaction coefficient becomes negligible. When the solubility $s$ was given in mol dm$^{-3}$ it was converted to molality basis with the well-known relationship

$$\lim_{c\to 0}\left(\frac{c}{m}\right) = \rho^*/\text{kg dm}^{-3} \quad (9)$$

where $\rho^*$ is the density of pure water. In Fig. 1, the solubility product of silver molybdate lg $K_{s0}^{\circ}$ has been plotted vs. 1000 K/$T$. Only the datum of Britton and German [3] is a conspicuous outlier and can be rejected safely. Mean values and uncertainties were calculated for each temperature for which two

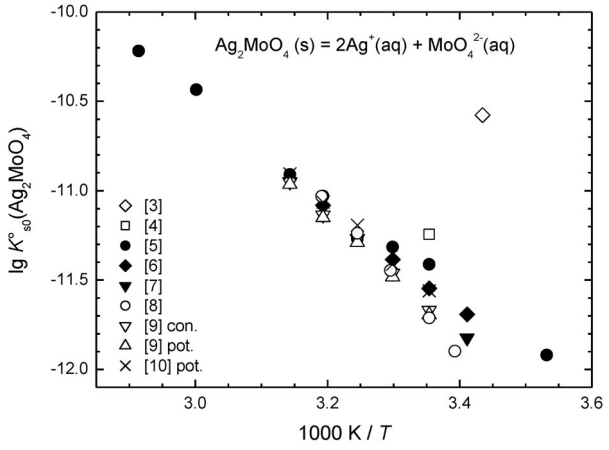


**Fig. 1** Solubility product of silver molybdate.

or more lg $K^{\circ}_{s0}$ values were determined. The highest uncertainty observed was assigned to single values also. Subsequently, these data were subjected to a weighted linear regression.

By this procedure (see Fig. 2), a value of lg $K^{\circ}_{s0}$ (298.15 K) has been obtained, which is comparatively robust and so is $\Delta_{sln}G^{\circ}$ of the corresponding dissolution reaction, eq. 1 (M = Ag, $n$ = 2). $\Delta_{sln}G^{\circ}$ is referenced to Henry's law, molality basis, see ref. [13] (definition of activity coefficient). Its value at 298.15 K is absolutely necessary for the calculation of $\Delta_f G^{\circ}$ ($MoO_4^{2-}$).

Clearly, $\Delta_{sln}H^{\circ}$ and $\Delta_{sln}S^{\circ}$ calculated from slope and intercept of lg $K^{\circ}_{s0}$ vs. 1000 K/$T$ plots are far less precise, but may be used for the calculation of $\Delta_f H^{\circ}$ ($MoO_4^{2-}$) and $\Delta_f S^{\circ}$ ($MoO_4^{2-}$) (Table 1).

**Table 1** Thermodynamic data of eq. 1 (M = Ag, $n$ = 2) at 298.15 K.

| |
|---|
| lg $K^{\circ}_{s0}$ = − (11.59 ± 0.05) |
| $\Delta_{sln}G^{\circ}$ = (66.16 ± 0.30)/kJ·mol$^{-1}$ |
| $\Delta_{sln}H^{\circ}$ = (58.4 ± 3.7)/kJ·mol$^{-1}$ |
| $\Delta_{sln}S^{\circ}$ = − (26.0 ± 11.7)/J·K$^{-1}$·mol$^{-1}$ |

The solubility product of $BaMoO_4$ according to eq. 1 (M = Ba, $n$ = 1) was determined for the first time by Rao [14,15], as experimental details are lacking the value reported [lg $K_{s0}$ ($BaMoO_4$) = −7.47] was not considered any further. The same is true for [lg $K_{s0}$ ($SrMoO_4$) = −6.59] [15]. The experimental data of Nesmeyanov et al. [16] are the only ones permitting the determination of

$$\lg K^{\circ}_{s0} = \lg\left(a_{M^{2+}} a_{MoO_4^{2-}}\right) = \lg\left(m_{M^{2+}} m_{MoO_4^{2-}}\right) - 8D \tag{10}$$

at various temperatures, where M is Ba or Sr. Two papers have been found which reported more reliable values for the solubility of $BaMoO_4$(cr) at 25 °C. Jost [17] equilibrated $BaMoO_4$ in aqueous NaCl solution. The $MoO_4^{2-}$ content of the saturated solutions was determined by coulometric analysis and polarography. For re-evaluation these data were converted to the molality scale. Figure 3 shows that data at higher ionic strengths deviate from linearity, but both accepted SIT extensions eq. 11 [18] and eq. 12 [19] fit very well.

 

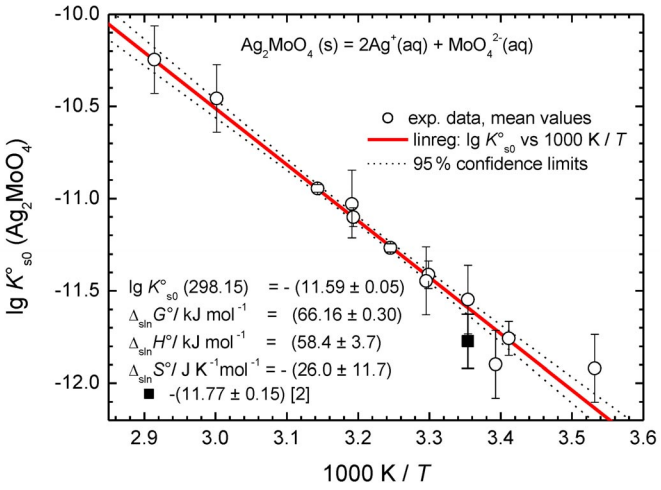


**Fig. 2** Thermodynamic analysis of solubility data.

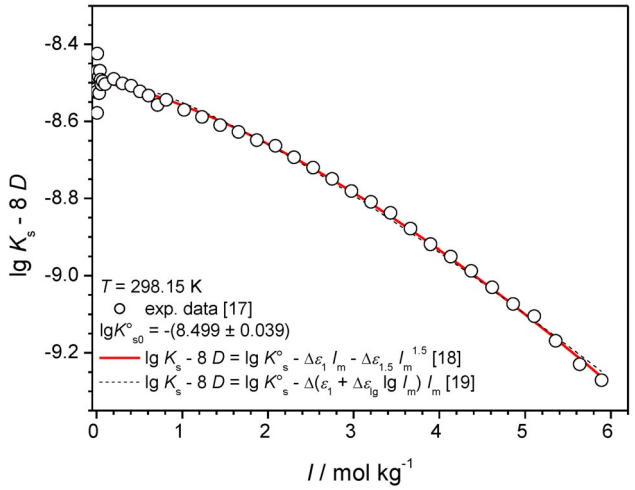


**Fig. 3** Solubility product of $BaMoO_4$(cr).

$$\lg K_{s0} - 8D = \lg K_{s0}^{\ominus} - \Delta\varepsilon_1 I_m - \Delta\varepsilon_{1.5} I_m^{1.5} \tag{11}$$

$$\lg K_{s0} - 8D = \lg K_{s0}^{\ominus} - (\Delta\varepsilon_1 + \Delta\varepsilon_{\lg}\ \lg I_m) I_m \tag{12}$$

$\Delta_{sln}G^{\ominus}$ [eq. 1 (M = Ba, $n$ =1), 298.15 K] = (48.512 ± 0.223) kJ·mol$^{-1}$

Çetin and Berkem [20] determined the solubility of $BaMoO_4$(cr) in water and aqueous solutions of KCl, $KClO_4$, $KNO_3$, KSCN, KBr, NaCl, LiCl, and $MgCl_2$ at ionic strengths from 0.025 to 0.12 M and at 25 °C by conductimetry. Solubility in pure water was also determined by atomic absorption and solution spectrometry. The mean value $\lg K_{s,m}^{\ominus} = -(8.51 \pm 0.15)$ agrees very well with the result of [17], but is less precise.

From the data of [16] the solubility product and the Gibbs energy of $SrMoO_4$(cr) dissolution have been calculated to be

$$\lg K^{\circ}_{s0}\ (SrMoO_4, cr, 298.15) = -(7.89 \pm 0.25)$$

$$\Delta_{sln}G^{\circ}\ [\text{eq. 1 (M = Sr, } n = 1), 298.15\ K] = (45.0 \pm 1.4)\ kJ{\cdot}mol^{-1}$$

Ten references have been found with experimental data seeming to permit the determination of the solubility product according to eq. 1 (M = Ca, $n$ = 1) covering a range of $-6.5 \geq \lg K^{\circ}_{s0} \geq -8.5$ at 25 °C. Dittler [21] determined the solubility of $CaMoO_4$ for the first time. The value reported leads to $\lg K_{s0}$ (30 °C) = −6.47, which seemed to be far too high and was not considered any further. The same is true for Zelikman and Prosenkova's $\lg K_{s0}$ values [22]. Spitsyn and Savich [23,24] and probably Nesmeyanov et al. [16] determined the solubility product of a calcium molybdate with the stoichiometric formula $CaMoO_4{\cdot}0.5H_2O$. This phase is obviously not identical with powellite. $CaMoO_4$(powe) has been investigated by Zhidikova and Khodakovskii [25], Zhidikova and Malinin [26], Essington [27], Grambow et al. [28], and Felmy et al. [29]. Grambow et al. [28] report that their phase dissolved incongruently and had the stoichiometric composition $CaMoO_4{\cdot}0.2H_2O$, but exhibited only the X-ray patterns of powellite before and after the dissolution experiment. The dependence of $\lg K^{\circ}_{s0}$ ($CaMoO_4$) on temperature determined by [16,26,28] is difficult to interpret and seems to indicate a phase transition. Thus, a reliable estimation of $\Delta_{sln}H^{\circ}$ and $\Delta_{sln}S^{\circ}$ cannot be made. For $\Delta_{sln}G^{\circ}$, the values reported by [26–29] were accepted, because in these contributions the solid phases investigated were characterized as $CaMoO_4$, powellite. The weighted mean of $\lg K^{\circ}_{s0}$ and $\Delta_{sln}G^{\circ}$ with uncertainties estimated by the author is listed in Table 2.

**Table 2** Solubility product $\lg K^{\circ}_{s0}$ ($CaMoO_4$, powe, 298.15 K).

| | $\lg K^{\circ}_{s0}$ | $\pm$ dlg $K^{\circ}_{s0}$ | References |
|---|---|---|---|
| | −8.33 | 0.20 | [26] |
| | −8.05 | 0.10 | [27] |
| | −7.95 | 0.10 | [28] |
| | −7.93 | 0.10 | [29] |
| Weighted mean | −8.004 | 0.055 | |
| $\Delta_{sln}G^{\circ}$/kJ·mol$^{-1}$ | 45.69 | 0.32 | |

### *Solubility product based on electrochemical data*

Pan [6] determined the standard solubility product according to eq. 1 (M = Ag, $n$ = 2) by an electrochemical method, which deserves to be outlined concisely (Fig. 4). The following galvanic cell was employed:

$$\begin{array}{l} Ag|Ag_2MoO_4(s)|\ Na_2MoO_4(\chi m)\ \|KNO_3(m)\|\ \ AgNO_3(3\chi m)\ \ |Ag_2MoO_4(s)|Ag, \\ \qquad\qquad\quad |NaNO_3(m{-}3\chi m)\|\qquad\quad \|NaNO_3(m\ {-}3\chi m)| \end{array} \qquad \text{(I)}$$

$m$ denotes molality, and $\chi$ is a fraction. The experimental data obtained with cell I have been evaluated by the method of double extrapolation. This approach is particularly useful for electrolytes of very low solubility for which direct measurements of solubility are difficult to come by [30].

On average, the cell potentials were reproducible within ±1 mV. Measurements were carried out at four different fractions $\chi$ (0.3, 0.2, 0.1, 0.05) to eliminate the liquid-junction potentials, at four different molalities $m$ (0.05, 0.04, 0.03, 0.02) to extrapolate to zero ionic strength, and at four different temperatures (20, 25, 30, 40 °C) to obtain the standard values for Gibbs energy, enthalpy, and entropy of silver molybdate dissolution according to reaction 10.

 

In order to eliminate the liquid-junction potentials, each series of measurements at constant $m$ has to be extrapolated to $\chi = 0$, see eqs. 13 and 14. For the extrapolation to ionic strength zero, the SIT method has been applied, as usual in this review, see eqs. 15 and 16.

$$2FE_I / RT \ln(10) - \lg\left[3^2 \cdot (\chi \cdot m)^3\right] = -\lg K'_{s0}(\chi) \tag{13}$$

$$\lg K'_{s0} = \lg K_{s0} + C \cdot \chi \tag{14}$$

$$\lg K_{s0} + \lg\left[\gamma^2_{Ag^+} \cdot \gamma_{MoO_4^{2-}}\right] = \lg K^{\ominus}_{s0} \tag{15}$$

$$\lg K_{s0} - 6D = \lg K^{\ominus}_{s0} - \Delta\varepsilon \cdot m \tag{16}$$

$$E^{\ominus}_I = -\left[RT \ln(10)/2F\right] \lg K^{\ominus}_{s0} \tag{17}$$

The recalculation showed that the data of [6] provide a reliable basis for the determination of $\Delta_{sln}G^\circ$ of reaction 10. The measurements were carried out at rather low ionic strengths, thus it does not make much difference whether the Debye–Hückel limiting law [6] or the SIT approach [11,12] is applied for their interpretation. The values for $\Delta_{sln}H^\circ$ and $\Delta_{sln}S^\circ$ are clearly less precise as they are not directly measured by this method, but obtained by calculus from the appropriate functions of temperature. This investigation has been carried out at four different temperatures only, thus more than two fit parameters of the functions $E^{\ominus}_I(T)$ and $\lg K^{\ominus}_{s0}(T)$ are not justified. For the determination of the standard entropy of dissolution in the temperature range $293.15 \le T/K \le 313.15$ $E^{\ominus}_I(T)$ has been regressed vs. $T$, $\Delta_{sln}S^{\ominus} = -2F(\partial E^{\ominus}/\partial T)_p$ thus obtained overlaps with that listed in Table 1. The latter was accepted, however, as more experimental data in a larger temperature range contributed to this value, see Fig. 2.

## From solubility data to phase diagrams

According to refs. [11,12], thermodynamically based fitting equations $Y[x(T)]$ can be derived from solubility data of anhydrous salts using ionic mole fractions as variables:

$$Y[x(T)] = \ln(x_+^{\nu_+} x_-^{\nu_-}) = -\Delta_{sln}G^{\ominus}_x(T)/RT - \ln f_\pm^{\nu} \tag{18}$$

where $\nu$ is the sum of stoichiometric numbers of ions in a salt and

$$\nu_\pm = (\nu_+^{\nu_+} \nu_-^{\nu_-})^{1/\nu} \tag{19a}$$

$$f_\pm = (f_+^{\nu_+} f_-^{\nu_-})^{1/\nu} \tag{19b}$$

$$x_+ = \nu_+ x / [1 + (\nu - 1)x] \tag{19c}$$

$$x_- = \nu_- x / [1 + (\nu - 1)x] \tag{19d}$$

$\Delta_{sln}G^{\circ}_x$ is referenced to Henry's law mole fraction basis, see ref. [13] (definition of activity coefficient). Inspection of eqs. 3–5 immediately reveals that the numerical values of $\Delta_{sln}G^{\circ}$ and $\Delta_{sln}S^{\circ}$ on mole fraction and molality basis differ, whereas the numerical value of $\Delta_{sln}H^{\circ}$ remains invariant against this change of composition variables.

In the pertinent case

$$Y(x) = 3\ln\left[\frac{4^{1/3} x_{Ag_2MoO_4}}{(1 + 2x_{Ag_2MoO_4})}\right] \tag{20}$$

According to Fig. 2, lg $K^{\circ}_{s0}$ depends linearly on $1/T$, consequently, eq. 21 will be an appropriate fitting function

$$Y(T) = a + b\ (\mathrm{K}/T) \tag{21}$$

From eqs. 20 and 21 follows eq. 22, where $x = x_{Ag_2MoO_4}$:

$$T\ /\ \mathrm{K} = \frac{b}{3\ln[4^{1/3}x/(1+2x)] - a} \tag{22}$$

Parameters $a$ and $b$ have been obtained by nonlinear regression, see Fig. 5. The fitted function $T(x)$ provides the basis for a partial phase diagram of the system $Ag_2MoO_4 + H_2O$, quite similar to systems of highly soluble salts + water [31].

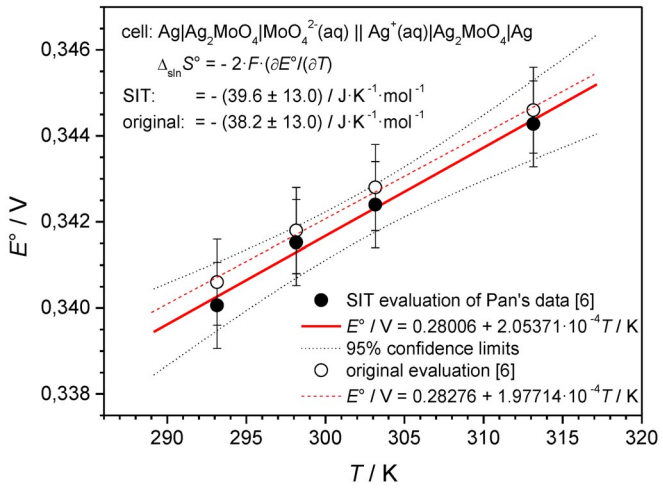


**Fig. 4** $E$: $Ag_2MoO_4(cr) = 2Ag^+(aq) + MoO_4^{2-}(aq)$.

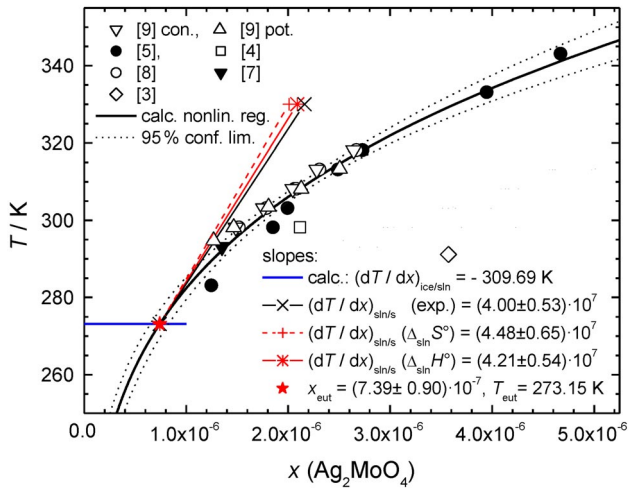


**Fig. 5** Partial phase diagram $Ag_2MoO_4 + H_2O$.

 

A eutectic point is located at the intersection of freezing point depression and solubility curves. In the present case, where the $x$ values are rather low, the theoretical limiting slope, $\sigma_{ice/sln}$ for the 1-2 charge type electrolyte (ionic mole fraction basis) coincides with the freezing point depression curve

$$T_{fus}^{ice} - T = -\frac{3RT_{fus}^{ice}}{\Delta_{fus}S_W^{\ominus}} \cdot x \tag{23}$$

where $\Delta_{fus}S_W^{\circ}/R = 2.646$ [32].

Solving eqs. 22 and 23 simultaneously results in $T_{eut}$ and $x_{eut}$, see Fig. 5. The slope d$T$/d$x$ along the solubility curve at the eutectic point can be observed experimentally and calculated theoretically.

$$\left(\frac{\mathrm{d}\,T}{\mathrm{d}\,x}\right)_{exp} \Big/ \mathrm{K} = \frac{\mathrm{d}Y(x)}{\mathrm{d}x} \cdot \frac{\mathrm{d}T}{\mathrm{d}Y(T)} = -\frac{3(T/\mathrm{K})^2}{x(1+2x)b} \tag{24}$$

$$\left(\frac{\mathrm{d}T}{\mathrm{d}x}\right)_{\Delta_{sln}H^{\ominus}} \Big/ \mathrm{K} = \sigma_{sln/S} = \frac{\nu(T/\mathrm{K})}{x[1+(\nu-1)x][\Delta_{sln}H^{\ominus}/RT - \nu T(\mathrm{d}\,\ln f_{\pm}/\mathrm{d}T)]} \tag{25}$$

$$\left(\frac{\mathrm{d}T}{\mathrm{d}x}\right)_{\Delta_{sln}S^{\ominus}} \Big/ \mathrm{K} = \sigma_{sln/S} = \frac{(T/\mathrm{K})\left\{\dfrac{\nu}{x[1+(\nu-1)x]}\right\}}{\Delta_{sln}S_x^{\ominus}/R - \nu\,\ln\left\{\dfrac{\nu_{\pm}x}{1+(\nu-1)x}\right\} - \nu\dfrac{\mathrm{d}(T\,\ln f_{\pm})}{\mathrm{d}T}} \tag{26}$$

Note that $\Delta_{sln}S_x^{\circ}/R = \Delta_{sln}S_m^{\circ}/R + \nu\ln(M_{H_2O}/m^{\circ})$, where $m^{\circ} = 1$ mol kg$^{-1}$ is the standard molality. The $f_{\pm}$ term has been neglected in eqs. 25 and 26 and $\Delta_{sln}S_m^{\circ}/R$ has been assumed to remain constant in the range between the eutectic temperature (273.15 K) and the standard temperature (298.15 K). Values for $\Delta_{sln}H^{\circ}$ and $\Delta_{sln}S^{\circ}$ have been taken from Wagman et al. [33]. Theoretical and experimental slopes agree within the experimental uncertainty and have a similar relative uncertainty of ±13–14 %, see Fig. 5. Thus, the thermodynamic interpretation of the experimental solubility data on silver molybdate is justified and the slope from the eutectic point along the solubility curve can be predicted directly, even when the $f_{\pm}$ term was neglected. In the case of highly soluble salts and salt hydrates an unknown $f_{\pm}$ term prevents the direct prediction of this slope, but may allow an approximate estimation of slope ratios [31].

### Calculation of $\Delta_f G^{\circ}$ ($MoO_4^{2-}$, aq) and $\Delta_f H^{\circ}$ ($MoO_4^{2-}$, aq)

In order to calculate $\Delta_f G^{\circ}$ ($MoO_4^{2-}$, aq) using eq. 2a, the standard Gibbs energies of formation for $M_nMoO_4$(cr) and $M^{2+/n}$(aq) are needed. $\Delta_f G^{\circ}$ values for the molybdates of silver, barium, and calcium can be taken from [33] directly. $\Delta_f G^{\circ}$ ($SrMoO_4$, cr) was calculated using the relationship $G = H - TS$. $\Delta_f H^{\circ}$ ($SrMoO_4$, cr) is listed in [33] and $\Delta_f S^{\circ}$ ($SrMoO_4$, cr) is available via the standard entropies listed by CODATA [34] (Sr(s), $O_2$), the NIST-JANAF Thermochemical Tables [35] (Mo(s)) and Kubaschewski et al. [36] ($SrMoO_4$, cr). $\Delta_f G^{\circ}$ ($M^{2+/n}$) values and their uncertainties have been taken from NEA auxiliary data, see e.g., [37]. The uncertainties assigned to Wagman et al.'s data [33] have been estimated by the author. By this procedure, the value $\Delta_f G^{\circ}$ ($MoO_4^{2-}$, aq) = −(835.32 ± 1.56) kJ·mol$^{-1}$ has been obtained, see Table 3. O'Hare et al. [2] arrived at a quite similar result $\Delta_f G^{\circ}$ ($MoO_4^{2-}$, aq) = −(836.8 ± 1.3) kJ·mol$^{-1}$.

For the evaluation of $\Delta_f H^{\circ}$ ($MoO_4^{2-}$, aq) and $S^{\circ}$ ($MoO_4^{2-}$, aq) using eqs. 2b and c the solubility data of silver molybdate are qualified only, see Table 3. The result for $\Delta_f H^{\circ}$ ($MoO_4^{2-}$, aq) agrees perfectly with the value listed in [33], and the uncertainty range of $\Delta_f S^{\circ}$ ($MoO_4^{2-}$) covers the value listed in [33].

**Table 3** Standard thermodynamic data of $MoO_4^{2-}$ at $T$ = 298.15 K, eqs. 2a–c.

| M, $n$ | $\Delta_{sln}G^\circ$/kJ·mol$^{-1}$ | Refs. | $n\,\Delta_fG^\circ$ ($M^{2+/n}$) | $\Delta_fG^\circ$ ($MoO_4^{2-}$) | $\Delta_fG^\circ$ ($M_nMoO_4$) | Refs. |
|---|---|---|---|---|---|---|
| Ag, 2 | 66.16 ± 0.30 | this work | 154.19 ± 0.31 | –836.03 ± 3.53 | –748.00 ± 3.50 | [33] |
| Ba, 1 | 48.51 ± 0.22 | [17] | –557.66 ± 2.58 | –833.43 ± 3.60 | –1439.60 ± 2.50 | [33] |
| Sr, 1 | 45.00 ± 1.40 | [16] | –563.86 ± 0.78 | –834.31 ± 4.02 | –1443.17 ± 3.68 | [33–36] |
| Ca, 1 | 45.69 ± 0.32 | this work | –552.81 ± 1.05 | –836.10 ± 2.28 | –1434.60 ± 2.00 | [33] |
| | | | weighted mean: | –835.32 ± 1.56 | | |
| | $\Delta_{sln}H^\circ$/kJ·mol$^{-1}$ | | $\Delta_fH^\circ$ ($M^{2+/n}$) | $\Delta_fH^\circ$ ($MoO_4^{2-}$) | $\Delta_fH^\circ$ ($M_nMoO_4$) | |
| Ag, 2 | 58.40 ± 3.70 | this work | 215.58 ± 0.16 | –997.78 ± 4.16 | –840.60 ± 1.90 | [33] |
| | | | | –997.9 | | [33] |
| | $\Delta_{sln}S^\circ$/J·K$^{-1}$ mol$^{-1}$ | | $\Delta_fS^\circ$ ($M^{2+/n}$) | $\Delta_fS^\circ$ ($MoO_4^{2-}$) | $\Delta_fS^\circ$ ($M_nMoO_4$) | |
| Ag, 2 | –26.00 ± 11.70 | this work | 146.90 ± 0.80 | 40.10 ± 14.78 | 213.00 ± 9.00 | [33] |
| | | | | 27.2 | | [33] |

To conclude this section, four remarks seem appropriate.

1. Since O'Hare's seminal paper [2] no other sparingly soluble molybdates than those of silver, barium, strontium, and calcium have been investigated reliably enough to make use of eq. 2a let alone eqs. 2b and c. So far no definitive study of the solubility product for $FeMoO_4$(s) has been performed. The situation for lead molybdate $PbMoO_4$, wulfenite, has also not improved. The thermodynamically calculated and the experimentally determined solubility products still differ by 3 to 8 orders of magnitude, see Table 4.
2. If solubility products of two sparingly soluble metal molybdates are well established, as is the case with silver and barium molybdate, the difference of the standard Gibbs energies of formation is also well established and can be used as a consistency test.
3. Solubility measurements on barium and strontium molybdate in a range of temperatures between, for example, 10 to 90 °C, would contribute significantly to the knowledge of thermodynamic data for molybdate ion.
4. Grobler and Suri's [8] measurements on $CuMoO_4$(s) indicate retrograde solubility, see Fig. 6. It is recommended to reinvestigate this system, because the solid phase was characterized stoichiometrically but not structurally and $\Delta_fH^\circ$ ($CuMoO_4$, s) derived from [8] differs by 55 kJ mol$^{-1}$ from that listed in [33].

**Table 4** Solubility product of lead molybdate, eq. 1 (M = Pb, $n$ = 1).

| $T$/K | lg $K^\circ_{s0}$ | Comments | Refs. |
|---|---|---|---|
| 295 | –9.72 | Solubility and phototurbidimetric method | [38] |
| 298 | –9.17 | Polarographic method | [39] |
| "Room" | –11.48 | Inversion-polarographic method | [40] |
| 298.15 | –15.88 | Thermodynamic data | [33] |
| 298.15 | –15.99 | Thermodynamic data | [41] |
| 298 | –(12.91 ± 0.11) | $Pb^{2+}$ selective electrode | [42] |
| 298.15 | –(7.90 ± 0.02) | Conductimetric, spectrometric method | [20] |

 

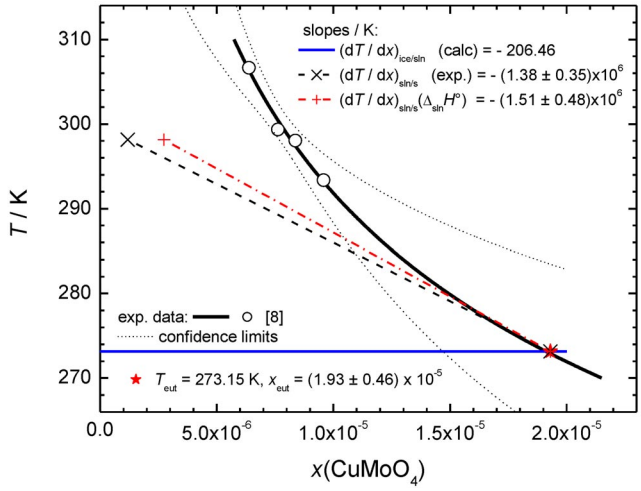


**Fig. 6** Partial phase diagram $CuMoO_4 + H_2O$.

## THERMODYNAMIC ANALYSIS OF THE SOLUBILITY OF SPARINGLY SOLUBLE IONIC SOLIDS WITH BASIC ANIONS

The determination of the solubility product of sparingly soluble ionic solids with basic anions is a straightforward method to evaluate the standard Gibbs energy of formation of the solid phase investigated. These solubility studies are characterized by the possibility to monitor the approach to equilibrium by measuring the pH. Methodological details of this field of research have been summarized by Gamsjäger and Königsberger [43]. A model study of the system $CdCO_3$(cr) + $CO_2$ (g) + $H_2O$ (l) has been published recently [44]. Here solubility studies of β-$Ni(OH)_2$ will be discussed, because they throw a new light on the most powerful criterion of equilibration.

### The elusive solubility constant of $Ni(OH)_2$

The published solubility products of nickel hydroxide show a scatter of at least three orders of magnitude, and the literature up to mid-2002 referring to this phenomenon has been reviewed by Gamsjäger et al. [45]. The aqueous solubility of β-$Ni(OH)_2$, theophrastite, is indeed difficult to determine, because the pH at saturation falls within the unbuffered range (pH ≈ 7), and $Ni^{2+}$ as well as β-$Ni(OH)_2$ are notoriously inert, thus at 25 °C equilibrium may not be attained within a period of three weeks. Mattigod et al. [46] were the first to investigate structurally well-defined samples and arrived at the same solubility from over- and undersaturation, which is the generally acknowledged criterion for equilibrium, see Fig. 7.

#### *Fractional dissolution*

An improved method to synthesize β-$Ni(OH)_2$ has been described by Gamsjäger et al. [47] and by Wallner and Gatterer [48]. It is based on the hydrolysis of sodium tetrahydroxoniccolate, $Na_2[Ni(OH)_4]$, and leads to pure macrocrystalline nickel(II) hydroxide with crystal sizes up to 0.2 mm. With this coarse crystalline material, solubility equilibria can only be attained from undersaturation, because large crystals of β-$Ni(OH)_2$ will not precipitate in the vicinity of equilibrium within typical experimental time periods. Thus, an invariant solubility constant over a broad range of starting conditions is the criterion for equilibration (pH variation method [49]). Whereas this method has often been successful, it seemed to be thermodynamically less rigorous than attaining equilibration from over- and undersaturation. In the present case, the solubility constant obtained for these large crystals was lower

by almost one order of magnitude than the one reported by Mattigod et al. [46] as illustrated in Figs. 8a and b.

Much to our disappointment, Don Palmer's results were closer to Mattigod et al.'s [46] than to ours. Don Palmer repeated his experiments, using β-$Ni(OH)_2$ samples provided by us, with his invincible hydrogen electrode concentration cell, which enables approach to equilibrium from over- and undersaturation. His lg* $K^{\circ}_{s0}$ values were still about 0.6 lg $K$ units higher than ours. As this difference exceeds the usual experimental error, the solubility of β-$Ni(OH)_2$(cr) was reinvestigated by the method of fractional dissolution. Batches of synthesized microcrystalline β-$Ni(OH)_2$ were reacted with $HClO_4/NaClO_4$ solutions of constant ionic strength until the pH remained constant. The reaction temperature was kept at 50 and 80 °C, respectively. After metastable or stable solubility equilibrium (indicated by a constant pH) was attained, the majority of the saturated solution was removed from the reaction vessel, analyzed for Ni(II), and replaced by the same volume of solution. This procedure was repeated until successive final pH values agreed with each other within experimental error limits. The

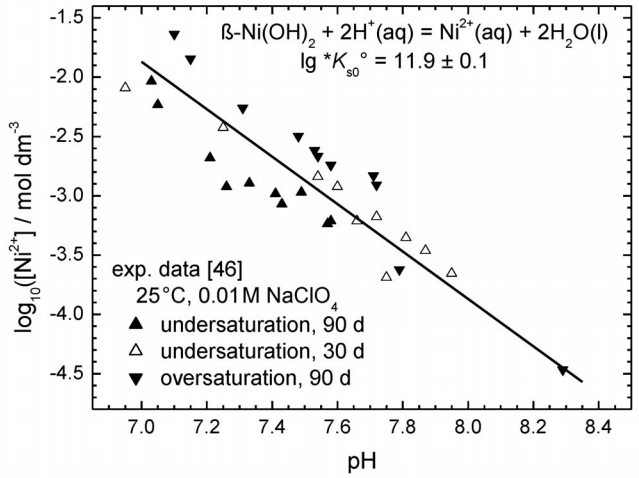


**Fig. 7** Solubility of β-$Ni(OH)_2$, theophrastite.

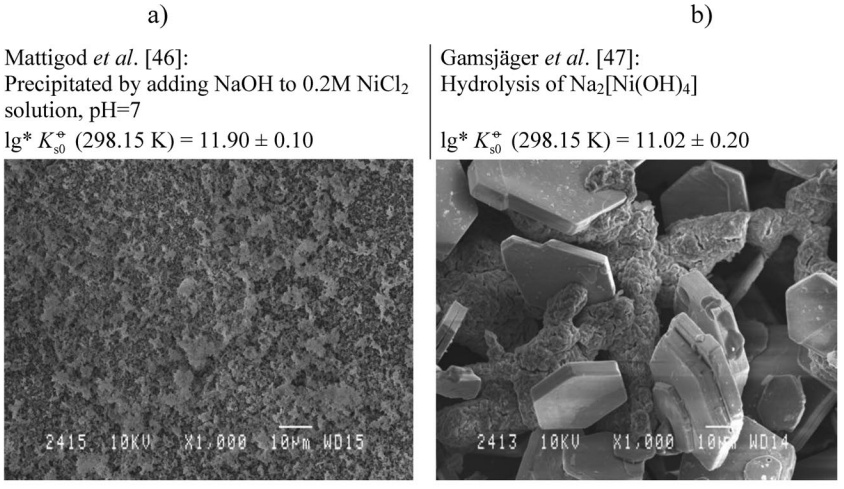


**Fig. 8** SEM image of β-$Ni(OH)_2$.

samples were inhomogeneous with respect to the dissolution reaction, but arrived at a stable equilibrium state after the mole fraction of dissolved β-$Ni(OH)_2$(cr) approached 0.25 to 0.3, see Fig. 9.

Scanning electron microscopy (SEM) images in Figs. 10a and b of samples taken before and after dissolution show that the finely dispersed particles had disappeared. These experiments were included in a paper by Palmer and Gamsjäger [50].

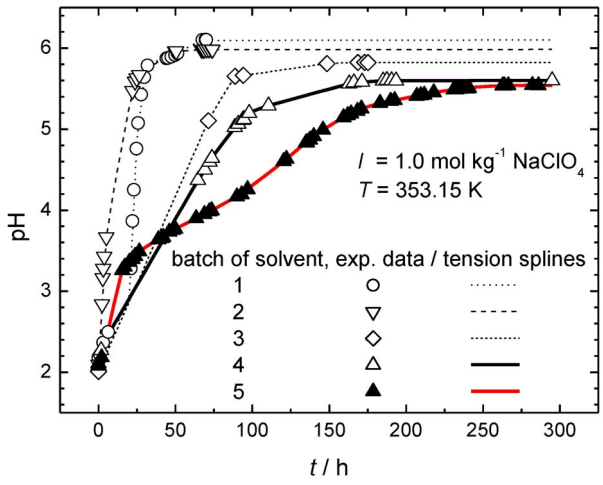


**Fig. 9** Fractional dissolution of β-$Ni(OH)_2$, pH = f(*t*).

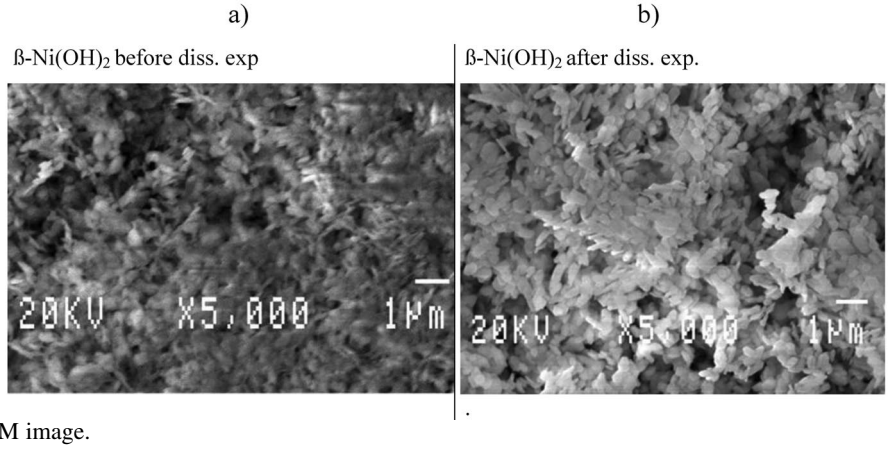


**Fig. 10** SEM image.

## Semi-theoretical estimation of surface tension

Elementary thermodynamic reasoning reveals that the difference in the Gibbs energy of dissolution of finely divided and coarse Ni(II) hydroxide is proportional to the molar surface tension $\gamma$. Thus, the molar surface can be estimated from the difference of the logarithmic solubility constants of fine and coarse material once the surface tension is known (Table 5).

**Table 5** Estimated molar surfaces of equilibrated β-$Ni(OH)_2$ fractions.

| 323.15 K | | 353.15 K | |
|---|---|---|---|
| $\Delta lg^*K_{s0}$ ± 0.2 | $A_m/m^2 \cdot mol^{-1}$ ± 4000 | $\Delta lg^*K_{s0}$ ± 0.2 | $A_m/m^2 \cdot mol^{-1}$ ± 4000 |
| 1.28 | 24 000 | 1.07 | 22 000 |
| 0.91 | 17 000 | 0.86 | 17 000 |
| 0.75 | 14 000 | 0.49 | 9900 |
| 0.62 | 11 000 | | |

The semi-theoretical estimation of the molar surface $A_m$ proposed by Schindler [51] was applied.

$$A_m = (3/2) \cdot RT\,[\ln K_{s0}(A_m) - \ln K_{s0}(A_m \to 0)]/\gamma \quad (27)$$

$$\beta\text{-}Ni(OH)_2(s) = Ni^{2+}(aq) + 2OH^-(aq)\ (K_{s0}) \quad (28)$$

Reversible pulverization:

$$\Delta_{sln}G^\circ{}_m(\text{eq. } 28) = -RT \ln K_{s0}(A_m \to 0) = (2/3) \cdot \gamma \cdot A_m \quad (29)$$

$$A_m = 4\pi L \cdot [r^2(Ni^{2+}) + 2 \cdot r^2(OH^-)] \quad (30)$$

In eq. 30, $r(Ni^{2+})$ and $r(OH^-)$ are the ionic radii and $L$ is the Avogadro constant.

$$\gamma = -1.5 \cdot RT \cdot \ln K_{s0}(A_m \to 0)/\{4\pi L \cdot [r^2(Ni^{2+}) + 2 \cdot r^2(OH^-)]\} \quad (31)$$

Equation 31 leads to

$$\gamma \approx (0.50 \pm 0.05)\ J \cdot m^{-2}$$

This semi-theoretically derived surface tension $\gamma$ of β-$Ni(OH)_2$ leads to estimates of molar surfaces $A_m$ which are comparable with those estimated from the particle sizes of Sorai et al.'s [52] nickel hydroxide samples. At $A_m \approx 1000\ m^2\ mol^{-1}$, measured $^*K_{s0}(A)$ values become indistinguishable.

### *Experimental consideration concerning particle size effects*

Solubility of β-$Ni(OH)_2$ is determined by the smallest particles present. The same equilibrium value from over- and undersaturation can be obtained only when sizes of dissolving and precipitating particles are similar.

Oswald and Asper [53] pointed out "that β-$Ni(OH)_2$ has often been described as a gel-like or amorphous phase, but is in reality always microcrystalline, although with a more or less disordered lattice. The extraordinarily small tendency of $Ni(OH)_2$ to form larger, well-shaped crystallites can be illustrated by comparison of electron microscopical pictures of fresh and aged precipitates. After 30 days at 70 °C under the mother liquor, extremely thin irregularly contoured platelets of a few 100 Å in diameter only are visible. Upon doubling the period of aging, no apparent increase in crystallinity occurs. $Mn(OH)_2$ crystallizes much more readily. The difference in solubilities cannot serve as a sufficient explanation, which must be sought instead in a specific kinetic hindrance of $Ni(OH)_2$ recrystallization in aqueous media."

## Criteria for solubility equilibria

The phenomenon described in the section **"**Experimental consideration concerning particle size effects" leads to second thoughts about the most rigorous criterion for equilibration.

1. Attainment of solubility equilibrium from over- and undersaturation leads, in the case of β-$Ni(OH)_2$, to particles with a molar surface $A_m \approx 10^4$ $m^2$ $mol^{-1}$. These particles are more soluble by $\Delta \lg^* K_{s0} \approx 0.6$ than coarser ones ($A_m < 4 \cdot 10^3$ $m^2$ $mol^{-1}$).
2. With coarse crystalline β-$Ni(OH)_2$ solubility equilibrium can only be attained from undersaturation. Thus, an in-variant solubility constant over a broad range of starting conditions is the criterion for equilibration ("pH variation method", P. Schindler [49]).

## POTENTIOMETRIC INVESTIGATION OF HYDROLYSIS REACTIONS IN THE SYSTEM Cr(III) + $H_2O$

A major disadvantage of many interesting dissolution–precipitation reactions from the educational point of view is the slow equilibration. Exceptions are the hexaaqua ions of chromium, rhodium, and iridium, where homo- and heterogeneous hydrolysis reactions can be studied by experimentally simple titration techniques which enable the acquisition of a large amount of data in a single laboratory period. An experiment has been developed for the simultaneous determination of protonation and solubility constants relevant to hydrolysis processes in the system Cr(III) + $H_2O$. Enthalpies and entropies of reaction can be estimated from measurements in the limited range of temperature from 5 to 25 °C.

When the hydrolysis reactions of metal ions are discussed, three processes should be distinguished according to their markedly different reaction rates.

1. Fast protolysis reactions. In reactions A and B, for example, no ligand substitution takes place, and the rates have been found to be diffusion controlled or nearly so in the direction of negative Gibbs energy of reaction [54]

$$M(OH_2)_n^{z+} \rightleftarrows M(OH_2)_{n-1}(OH)^{(z-1)+} + H^+ \quad (A)$$

$$M(OH_2)_{n-1}(OH)^{(z-1)+} \rightleftarrows M(OH_2)_{n-2}(OH)_2^{(z-2)+} + H^+ \quad (B)$$

2. Condensation reactions which lead to dinuclear C and on to polynuclear μ-hydroxo complexes [55]. Ligand substitution processes of this kind are generally slower than proton-transfer reactions and will be particularly slow when substitution of inert hexaaqua Cr(III) ion is involved.

$$2(OH_2)_{n\text{-}1}(OH)^{(z-1)+} \rightleftharpoons (H_2O)_{n\text{-}2}M\begin{matrix} H \\ O \\ O \\ H \end{matrix}M(H_2O_2)_{n\text{-}2}^{2(z-1)+} + H_2O \quad (C)$$

3. Precipitation of solid oxides, hydroxides, and basic salts [49]. Frequently, equilibria of these heterogeneous processes are attained rather slowly and the stable state will be attained after periods of hours to years. However, Meyenburg et al. [56] found rapid equilibration for a heterogeneous hydrolysis reaction in the system Cr(III) + $H_2O$. The solid product was identified to be Cr(III)-trihydroxide–trihydrate [57], and it was concluded that the original coordination octahedrons are held together by hydrogen bonding in this compound. Thus, no ligand substitution processes are involved when the precipitate is formed.

The system Cr(III) + $H_2O$ was selected for the experiment developed here, because it is comparatively inexpensive, and a simultaneous investigation of homogeneous protolysis and heterogeneous precipitation equilibria seemed to be feasible in analogy to the system Ir(III) + $H_2O$ [58]. For the titration technique, the following cell II was used:

$$\begin{array}{l|l|l|l|l} \text{Pt, } H_2 & & & \text{NaCl (0.01 M)} & \\ \quad \text{or} & \text{test sln.} & NaClO_4 & & \text{Ag, AgCl} \\ \text{glass-el.} & & 1.0\ \text{M} & NaClO_4\,(0.90\ \text{M}) & \end{array} \quad (II)$$

The potential of cell II is given by the extended Nernst equation

$$E = E^{\circ} - (RT \ln(10)/F)\ \mathrm{pH} + E_j \tag{32}$$

where $E_j$ depends linearly on $[H^+]$. A numerical value for $E_j$ may be determined as part of the experiment by titrating $HClO_4$ with NaOH at constant ionic strength, e.g., 1.0 M $NaClO_4$. The electrode system can simply be calibrated with an acid solution of known composition and constant ionic strength. The following parameters have to be determined experimentally: $[Cr^{3+}]_{tot}$, the total acidity $H$, and the free $[H^+]$. These observables give $Z$, the average number of OH bound to Cr according to eq. 33

$$Z = ([H^+] - H)]/[Cr^{3+}]_{tot} \tag{33}$$

## Protolysis of $Cr(OH_2)_6^{3+}$, homogeneous range

In the homogeneous range, $Z$ can be expressed as

$$Z = \frac{[Cr(OH)] + 2[Cr(OH)_2]}{[Cr] + [Cr(OH)] + [Cr(OH)_2]} \tag{34}$$

where coordinated water and charges have been omitted for the sake of brevity. This leads to a relationship (34) which is independent of $[Cr^{3+}]_{tot}$.

$$Z = \frac{{}^*K_1[H^+]^{-1} + 2{}^*K_1{}^*K_2[H^+]^{-2}}{1 + {}^*K_1[H^+]^{-1} + {}^*K_1{}^*K_2[H^+]^{-2}} \tag{35}$$

The constants ${}^*K_1$ and ${}^*K_2$ in eq. 35 refer to the following protolysis equilibria:

$Cr(OH_2)_6^{3+} \rightleftharpoons Cr(OH_2)_5OH^{2+} + H^+$ ${}^*K_1$

$Cr(OH_2)_5OH^{2+} \rightleftharpoons Cr(OH_2)_4(OH)_2^{+} + H^+$ ${}^*K_2$

Figure 11 represents experimental results in the homogeneous range.

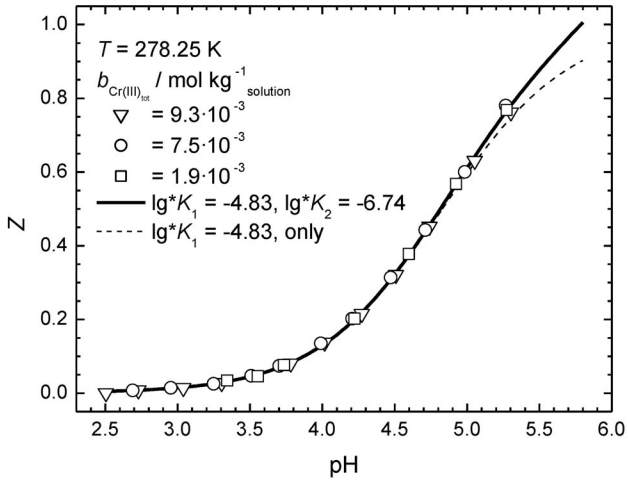


**Fig. 11** Protolysis of $Cr(OH_2)_6^{3+}$, homogeneous range.

### Protolysis of $Cr(OH_2)_6^{3+}$, heterogeneous range

If the only heterogeneous equilibrium involved is that given below

$$Cr(OH_2)_3(OH)_3(cr) + 3H^+ \Leftrightarrow Cr(OH_2)_6^{3+} \quad {}^*K_{s0}$$

$Z$ can be written as eq. 36

$$Z = \frac{[Cr(OH)] + 2[Cr(OH)_2] + 3[Cr(OH)_3]}{[Cr] + [Cr(OH)] + [Cr(OH)_2] + [Cr(OH)_3]} \tag{36}$$

where $[Cr(OH)_3]$ is the stoichiometric concentration of precipitated Cr(III) hydroxide and should not be confused with the uncharged species $Cr(OH)_3$. Insertion of equilibrium constants and rearrangement leads to

$$Z = \frac{{}^*K_{s0}[H^+]^3(3+2{}^*K_1[H^+]^{-1} + K_1{}^*K_2[H^+]^{-2})}{[Cr]_{tot}} \tag{37}$$

Once the constants controlling homogeneous protolysis equilibria are known, ${}^*K_{s0}$ can be evaluated from a plot of $Z$ against the composite variable $X$

$$X = \frac{[H^+]^3(3+2{}^*K_1[H^+]^{-1} + K_1{}^*K_2[H^+]^{-2})}{[Cr]_{tot}} \tag{38}$$

As shown in Fig. 12, $Z$ is indeed a function of $pX = -\lg X$ alone. The calculated curve shows satisfactory agreement with the experimental data even in the buffered region. Below 25 °C and up to $Z$ = 3, precipitation and redissolution are strikingly reversible and the equilibration rate is hardly slower than in the homogeneous range. Since Cr(III) species are notoriously inert, this implies that the solid hydrolysis product is formed without involving any ligand substitution processes, and consequently hydrogen bonding plays the crucial part in the precipitation and dissolution of this type of hydroxide $Cr(OH)_3 \cdot 3H_2O$.

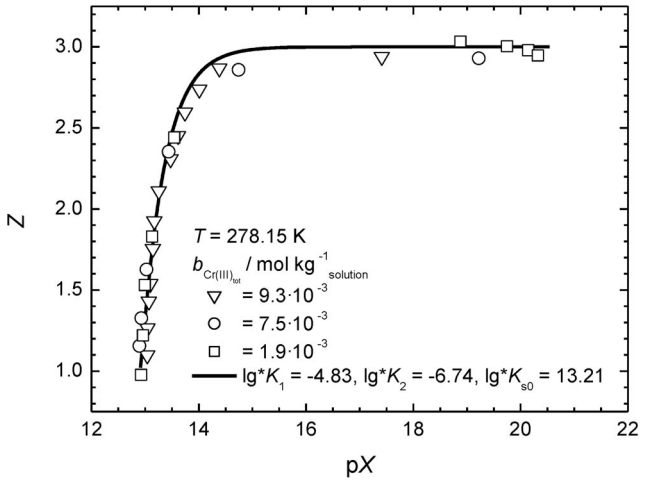


**Fig. 12** Protolysis of $Cr(OH_2)_6^{3+}$, heterogeneous range.

## CONCLUSIONS

- State-of-the-art solubility studies provide valuable data for thermodynamic databases.
- Thermodynamic analyses of solubility data guarantee the consistency of the quantities obtained within the framework of physical chemistry.
- There are experimentally and theoretically demanding examples that provide rewarding laboratory exercises for students.

## REFERENCES


1. P. A. O'Hare. *J. Chem. Thermodyn.* **6**, 425 (1974).
2. P. A. G. O'Hare, K. J. Jensen, H. R. Hoekstra. *J. Chem. Thermodyn.* **6**, 681 (1974).
3. H. T. S. Britton, W. L. German. *J. Chem. Soc.* 1156 (1934).
4. L. W. McCay. *J. Am. Chem. Soc.* **56**, 2548 (1934).
5. J. E. Ricci, W. F. Linke. *J. Am. Chem. Soc.* **73**, 3601 (1951).
6. K. Pan. *J. Chin. Chem. Soc.-Taip*., Ser. II 16 (1954).
7. R. Weiner, P. Boriss. *Fresenius' J. Anal. Chem.* **160**, 343 (1958), in German.
8. S. R. Grobler, S. K. Suri. *J. Inorg. Nucl. Chem*. **42**, 51 (1980).
9. M. Doğan, I. Ç. Sönmezoğlu. *Turk. J. Chem.* **16**, 223 (1992).
10. M. Doğan, I. Ç. Sönmezoğlu. *Kim. Kim. Muhendisligi Semp.*, 8$^{th}$, **3**, 39 (1992), in Turkish.
11. H. Gamsjäger, J. W. Lorimer, M. Salomon, D. G. Shaw, R. P. T. Tomkins. *Pure Appl. Chem.* **82**, 1137 (2010).
12. H. Gamsjäger, J. W. Lorimer, M. Salomon, D. G. Shaw, R. P. T. Tomkins. *J. Phys. Chem. Ref. Data* **39**, 02301 (2010).
13. H. Gamsjäger, J. W. Lorimer, P. Scharlin, D. G. Shaw. *Pure Appl. Chem*. **80**, 233 (2008).
14. D. V. R. Rao. *Curr. Sci. India* **22**, 274 (1953).
15. D. V. R. Rao. *J. Sci. Ind. Res. India* **13B**, 309 (1954).
16. A. N. Nesmeyanov, I. A. Savich, M. F. El'kind, V. Koryazhkin. *Vestnik Moskov Univ*. **11** (Ser. Mat., Mekh., Astron., Fiz., Khim. No. 1), 221 (1956), in Russian.
17. P. Jost. *Bull. Soc. Chim. Fr*. **51**, 2993 (1972), in French.
18. I. Grenthe, A. V. Plyasunov, K. Spahiu. "Estimations of medium effects on thermodynamic data", in *Modelling in Aquatic Chemistry*, I. Grenthe, I. Puigdomènech (Eds.), pp. 325–426, p. 347, Nuclear Energy Agency, OECD, Paris (1997).
19. L. Ciavatta. *Ann. Chim.-Rome* **70**, 551 (1980).
20. I. Çetin, A. R. Berkem. *Chim. Acta Turcica* **6**, 51 (1978), in French.
21. E. Z. Dittler. *Kristallogr. Mineral.* **54**, 332 (1914).
22. A. N. Zelikman, T. E. Prosenkova. *Russ. J. Inorg. Chem.* **6**, 105 (1961).
23. V. I. Spitsyn, I. A. Savich. *Russ. J. Gen. Chem*. **22**, 1323 (1952).
24. V. I. Spitsyn, I. A. Savich. *Russ. J. Inorg. Chem.* **3**, 351 (1958).
25. A. P. Zhidikova, I. L. Khodakovskii. *Geokhimiya* 427 (1971), in Russian.
26. A. P. Zhidikova, S. D. Malinin. *Geokhimiya* 28 (1972), in Russian.
27. M. E. Essington. *Environ. Sci. Technol*. **24**, 214 (1990).
28. B. Grambow, R. Müller, A. Rother. *Radiochim. Acta* **58** (Pt. 1), 71 (1992).
29. A. R. Felmy, D. Rai, M. J. Mason. *J. Solution Chem*. **21**, 525 (1992).
30. M. L. McGlashan. *Chemical Thermodynamics*, pp. 314–316, Academic Press, New York (1979).
31. H. Gamsjäger, J. W. Lorimer, E. Gamsjäger. *Monatsh. Chem*. **144**, 103 (2013).
32. E. W. Washburn. *International Critical Tables*, Vol. 5, pp. 95, 113, McGraw-Hill (1929).
33. D. D. Wagman, W. H. Evans, V. B. Parker, R. H. Schumm, I. Halow, S. M. Bailey, K. L. Churney, R. L. Nuttall. *J. Phys. Chem. Ref. Data* **11**, Suppl. 2 (1982).


 

34. J. D. Cox, D. D. Wagman, V. A. Medvedev. *CODATA Key Values for Thermodynamics*, Hemisphere, New York (1989).
35. M. W. Chase Jr. Monograph No. 9. NIST-JANAF Thermochemical Tables, *J. Phys. Chem. Ref. Data* (1998).
36. O. Kubaschewski, C. B. Alcock, P. J. Spencer. *Materials Thermochemistry*, 6th ed., Pergamon, Oxford (1993).
37. H. Gamsjäger, T. Gajda, J. Sangster, S. K. Saxena, W. Voigt. *Chemical Thermodynamics of Tin*, Nuclear Energy Agency Data Bank, Organisation for Economic Co-operation and Development (Ed.), Vol. 12, Chemical Thermodynamics, OECD Publications (2013). www.oecd-nea.org/dbtdb/pubs/tin.pdf
38. M. L. Chepelvetskii, K. F. Kharitonovich. *J. Anal. Chem. USSR* **18**, 314 (1963).
39. G. S. Deshmukh, R. K. Nandi. *Indian J. Chem.* **4**, 414 (1966).
40. E. M. Skobets, D. S. Turova, A. I. Karnaukhov. *Ukr. Khim. Zh.* **36**, 33 (1970) (Engl. ed.).
41. I. Dellien, K. G. McCurdy, L. G. Hepler. *J. Chem. Thermodyn.* **8**, 203 (1976).
42. E. E. Chao, K. L. Cheng. *Talanta* **24**, 247 (1977).
43. H. Gamsjäger, E. Königsberger. "Solubility of sparingly soluble ionic solids in liquids", in *The Experimental Determination of Solubilities*, G. T. Hefter, R. P. T. Tomkins (Eds.), pp. 315–358, John Wiley, Chichester (2003).
44. H. Gamsjäger, M. C. F. Magalhães, E. Königsberger, K. Sawada, B. R. Churagulov, P. Schmidt, D. Zeng. IUPAC-NIST Solubility Data series, 92. *J. Phys. Chem. Ref. Data* **40**, 043104 (2011).
45. H. Gamsjäger, J. Bugajski, T. Gajda, R. Lemire, W. Preis. "Chemical thermodynamics of nickel", in *Chemical Thermodynamics*, Nuclear Energy Agency Data Bank, OECD (Organisation for Economic Cooperation and Development) (Ed.), Vol. 6, North-Holland Elsevier, Amsterdam (2005).
46. S. V. Mattigod, D. Rai, A. R. Felmy, L. Rao. *J. Solution Chem.* **26**, 391 (1997).
47. H. Gamsjäger, H. Wallner, W. Preis. *Monatsh. Chem.* **133**, 225 (2002).
48. H. Wallner, K. Gatterer. *Z. Anorg. Allg. Chem.* **628**, 2818 (2002).
49. P. Schindler. *Chimia* **17**, 313 (1963).
50. D. A. Palmer, H. Gamsjäger. *J. Coord. Chem.* **63**, 2888 (2010).
51. P. W. Schindler. *Adv. Chem. Ser.* No. 67, 196 (1967).
52. M. Sorai, A. Kosaki, H. Suga, S. Seki. *J. Chem. Thermodyn.* **1**, 119 (1969).
53. H. R. Oswald, R. Asper. *Bivalent Metal Hydroxides, Preparation and Crystal Growth of Material with Layered Structures*, R. M. A. Lieth (Ed.), pp. 71–140, D. Reidel, Dordrecht (1977).
54. H. Strehlow, W. Knoche. *Fundamentals of Chemical Relaxation*, Monographs in Modern Chemistry 10, p. 70, Verlag Chemie, Weinheim (1977).
55. H. Wendt. *Chimia* **27**, 575 (1973).
56. U. Von Meyenburg, O. Sirokŷ, G. Schwarzenbach. *Helv. Chim. Acta* **56**, 1099 (1973).
57. R. Giovanoli, W. Stadelmann, W. Feitknecht. *Helv. Chim. Acta* **56**, 839 (1973).
58. H. Gamsjäger, P. Beutler. *J. Chem. Soc., Dalton Trans.* 1415 (1979).


 